July 30, 2008

Recirculation in multiple wave conversions

A. J. Brizard
Department of Chemistry and Physics, Saint Michael's College, Colchester, VT 05439

A. N. Kaufman
Lawrence Berkeley National Laboratory, University of California, Berkeley, CA 94720

E. R. Tracy
Department of Physics, College of William and Mary, Williamsburg, VA 23187-8795

A one-dimensional multiple wave-conversion model is constructed that allows energy recirculation in ray phase space. Using a modular eikonal approach, the connection coefficients for this model are calculated by ray phase-space methods. Analytical results (confirmed numerically) show that all connection coefficients exhibit interference effects that depend on an interference phase, calculated from the coupling constants and the area enclosed by the intersecting rays. This conceptual model, which focuses on the topology of intersecting rays in phase space, is used to investigate how mode conversion between primary and secondary waves is modified by the presence of a tertiary wave.

PACS numbers: 52.35.-g, 52.35.Hr, 52.35.Lv

I. INTRODUCTION

The process of mode conversion in a magnetized plasma, involving the interaction between two distinct propagating waves, represents an important mechanism by which rf heating and current drive may lead to a burning plasma [1]. According to a standard mode-conversion scenario for rf heating in a magnetized plasma, a primary (e.g., magnetosonic) wave carries rf power into the plasma until it is partially converted to a secondary (e.g., ion cyclotron) wave (see Fig. 1) from which the converted power is absorbed (which ultimately leads to plasma heating [2]). When a plasma contains multiple particle species, a variety of waves may interact resonantly, leading to the possibility of interesting interference effects. Given their potential complexity, it is desirable to investigate simplified models that capture the essence of the phenomena.

In the present work we investigate how a double conversion between primary and secondary plasma waves may be

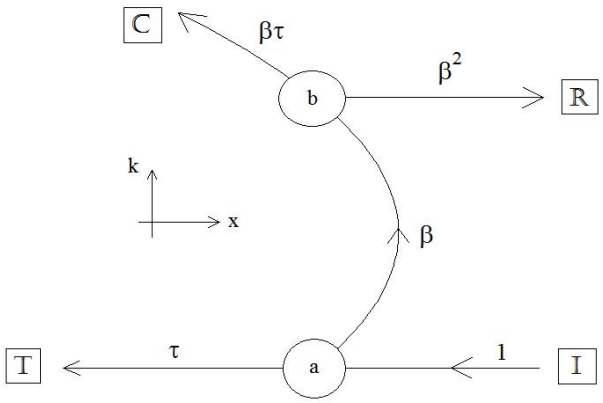

FIG. 1: Ray phase-space diagram for a double wave-conversion process with conversion regions a and b. Arrows indicate wave-packet propagation. The horizontal incident, transmitted, and reflected rays are associated with a bidirectional primary wave (e.g., magnetosonic) while the converted parabolic ray is associated with a unidirectional secondary wave (e.g., ion Bernstein). The single-conversion amplitude transmission and conversion coefficients are τ and β. The energy transmission, conversion, and reflection coefficients $\mathsf{T} = \tau^2$, $\mathsf{C} = |\beta|^2\,\tau^2$, and $\mathsf{R} \equiv |\beta^2|^2$ satisfy the energy conservation law $\mathsf{T} + \mathsf{C} + \mathsf{R} = 1$.

modified by a tertiary wave (perhaps supported by an energetic particle population). For this purpose, we develop a one-dimensional model that allows interference effects and energy recirculation. We note that this paper emphasizes the topology of intersecting rays that enclose area in two-dimensional phase space, and leave the ray geometry of specific plasma waves to future work.

Within this model, the transmission, reflection, and conversion coefficients are calculated by ray phase-space methods [3, 4] and a modular eikonal approach [5]. Analytical and numerical results show that these connection coefficients exhibit interference effects, which depend on an interference phase calculated from the coupling constants and the area enclosed by the rays.

The remainder of the paper is organized as follows. In Sec. II, we analyze the double-conversion model in order to introduce key ideas and useful notation associated with the modular eikonal approach. In Sec. III, we review previous works on multiple wave-conversions and introduce the two connection rules needed to perform the modular eikonal analysis of multiple wave-conversion problems that involve area enclosed by intersecting rays. In Sec. IV, we present a simplified one-dimensional model that enables us to focus our attention on the essence of interference and recirculation effects in ray phase space. A useful feature of this simplified model lies with the simple wave energy conservation law it possesses, which allows direct comparison with numerical analysis. We then solve our multiple wave-conversion model by using the modular eikonal approach [5–7] and construct the transmission and reflection coefficients associated with the primary wave, and the conversion coefficients associated with the secondary and tertiary waves. Here, the recirculation of wave energy introduces interference effects that depend on the pair-wise mode-coupling constant at each conversion point and the area enclosed by the intersecting rays.

In Sec. V, we compare the analytical results for the connection coefficients presented in Sec. IV with numerical results associated with the direct integration of the coupled-wave equations presented in Sec. IV. The excellent agreement found between the analytical and numerical results validates the use of the modular eikonal approach. In Sec. VI, we briefly discuss the possibility that, when the tertiary wave is supported by an inverted population of energetic particles, the tertiary-wave energy may be negative and thus the secondary-wave conversion coefficient may exceed unity. Lastly, we present our conclusions in Sec. VII and discuss applications and future work.

II. DOUBLE-CONVERSION MODEL

Before presenting our multiple wave-conversion model in Sec. IV, it is useful to review the ray phase-space analysis of single and double conversion processes [3]. In a standard single-crossing mode-conversion scenario (see conversion region a in Fig. 1), an incident ray from a primary wave propagates on its dispersion surface until it crosses (transversely) the dispersion surface of a secondary wave. Mode conversion occurs when some of the energy carried by a ray of the primary wave is converted to energy carried by a ray of the secondary wave, which allows the secondary ray to propagate away from the conversion region. The remaining energy associated with the primary wave is transmitted across the conversion region (by tunneling) and allows a primary-wave ray to propagate away from the conversion region.

Energy conservation dictates that the sum of the outgoing energy fluxes is equal to the sum of the incoming energy fluxes at each conversion region in ray phase space [8]. For each unit of energy entering a conversion region, the energy transmission coefficient is the square of the real-valued amplitude coefficient

$$\tau \;=\; \exp\left(-\,\epsilon\pi\;|\overline{\eta}|^2\right), \tag{1}$$

which is expressed in terms of the product ϵ of the wave-energy signs and the normalized coupling coefficient $\overline{\eta}$ (to be defined later). The energy conversion coefficient is the squared magnitude of the complex-valued amplitude conversion coefficient [3, 4]

$$\beta \;=\; \frac{(2\pi\,\tau)^{\frac{1}{2}}}{\overline{\eta}\;\Gamma(-i\,|\overline{\eta}|^2)} \;=\; \left(1-\tau^2\right)^{\frac{1}{2}}\;\exp(i\,\varphi), \tag{2}$$

where $\Gamma(z)$ denotes the gamma function and φ denotes the phase of β. These coefficients satisfy the single-conversion energy conservation law $\tau^2+|\beta|^2\equiv 1$.

The simplest double-conversion scenario in applications of rf power in magnetized plasmas is shown in Fig. 1, where energy from an incoming (bidirectional) primary wave (e.g., magnetosonic wave) is partially converted to a secondary wave located within a resonance layer (e.g., ion hybrid wave). Here, the unidirectional propagation of the secondary wave is due to nonuniformity in the plasma background. The remaining energy is divided between the primary-wave rays transmitted through the resonance layer (by tunneling) and reflected from the resonance layer.

In a nonuniform plasma with one-dimensional spatial dependence, the coupled-wave equations for a generic two-wave conversion process are given in matrix form as [3, 4]

$$\begin{pmatrix} D_A(x,\widehat{k}) & \eta \\ \eta^* & D_B(x,\widehat{k}) \end{pmatrix} \begin{pmatrix} A(x) \\ B(x) \end{pmatrix} \;=\; 0, \tag{3}$$

where $\widehat{k} = -i\,d/dx$, η denotes the coupling constant, and the complex-valued fields $A(x)$ and $B(x)$ represent the primary and secondary waves, respectively. Within the eikonal approximation (i.e., far away from a conversion region so that $\widehat{k} \to k$), the dispersion curve $x_j(k;\omega)$ for each wave is determined by $D_j(x,k;\omega) = 0$. Wave packets travel along dispersion curves according to Hamilton's ray equations

$$\left(\dot{x}_j,\; \dot{k}_j\right) \;\equiv\; \left(-\,\frac{\partial D_j}{\partial k},\; \frac{\partial D_j}{\partial x}\right), \tag{4}$$

where a dot refers to a derivative with respect to the ray parameter. In addition, the sign of the wave energy for each wave is determined by the sign of $\partial D_j/\partial\omega$ [6, 7].

In the wave equation (3), the primary wave (shown in Fig. 1) is modeled by its dispersion function $D_A(k) = k_0^2 - k^2$ so that $(\dot{x}_A, \dot{k}_A) = (\pm\,2k_0,\; 0)$ on the dispersion curves $k = \pm\,k_0$. The secondary wave (shown in Fig. 1), on the other hand, is modeled by its dispersion function $D_B(x,k) = x + \alpha\,k^2$ so that $(\dot{x}_B, \dot{k}_B) = (-\,2\alpha k,\; +1)$ on the dispersion curve $x(k) = -\,\alpha\,k^2$. Using these dispersion functions, the energy-flux conservation law

$$0 \;=\; \frac{d}{dx}\,[J_A(x) + J_B(x)]$$

becomes

$$0 \;\equiv\; \frac{d}{dx}\left[\;\mathrm{Im}\left(A^*\,\frac{dA}{dx}\right) \;-\; \alpha\;\mathrm{Im}\left(B^*\,\frac{dB}{dx}\right)\;\right], \tag{5}$$

where $J_j(x)$ denotes the energy flux of wave $j = A, B$. Note that, in the limit $\alpha \to 0$, the wave equation (3) yields the standard Budden equation [3]

$$\frac{d^2A(x)}{dx^2} \;+\; \left(k_0^2 \;-\; \frac{|\eta|^2}{x}\right) A(x) \;=\; 0, \tag{6}$$

where the secondary field $B(x) = -\,\eta^* A(x)/x$ is singular at $x = 0$ (i.e., B-wave rays propagate only in k-space).

The ray phase-space analysis of the double-conversion process involving primary and secondary positive-energy waves ($\epsilon = +1$) proceeds through a modular eikonal approach as follows. First, an incoming primary ray (traveling in x-space only) is converted to a secondary ray at the first conversion region a. Next, the secondary ray propagates in (x,k)-space to the second conversion region b where it is converted to an outgoing (reflected) primary ray and an outgoing (transmitted) secondary ray. For each unit of energy in the primary ray incoming at the conversion region a, the transmitted energy carried by the outgoing primary ray is

$$\mathsf{T} \;\equiv\; \tau^2 \;=\; \exp\left(-\,2\pi\;|\overline{\eta}|^2\right) \;<\; 1, \tag{7}$$

while the converted energy carried by the secondary ray is represented by the complex-valued conversion amplitude β. At the second conversion region b, the transmitted energy carried by the secondary ray is

$$\mathsf{C} \;\equiv\; |\beta|^2\,\tau^2 \;=\; \tau^2\,\left(1 \;-\; \tau^2\right), \tag{8}$$

while the converted energy carried by the outgoing (reflected) primary ray is

$$\mathsf{R} \;\equiv\; |\beta^2|^2 \;=\; \left(1 \;-\; \tau^2\right)^2. \tag{9}$$

The connection coefficients (7)-(9) satisfy the double-conversion energy conservation law

$$1 \;=\; \mathsf{T} + \mathsf{C} + \mathsf{R}, \tag{10}$$

which follows from the conservation law (5).

Lastly, we note that if the secondary wave has negative energy [9] (e.g., a minority-ion Bernstein wave supported by an inverted population of energetic particles [10, 11]), the transmission amplitude (1) is now $\tau = \exp(+\,\pi\;|\overline{\eta}|^2) > 1$ and the phase $\varphi = \arg(\beta)$ is replaced with $-\,\varphi$. These replacements imply that the transmission coefficient $\mathsf{T} = \tau^2 > 1$, the conversion coefficient $\mathsf{C} = -\,\tau^2\,\left(\tau^2 - 1\right) < 0$ (as is required for energy conversion between a positive-energy wave and a negative-energy wave), and the reflection coefficient $\mathsf{R} = \left(\tau^2 - 1\right)^2$ still satisfy the energy conservation law (10).

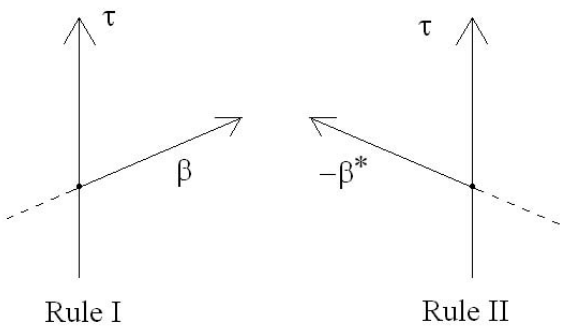

FIG. 2: Connection rules I and II for a single-crossing mode conversion. At each conversion point, τ denotes the real-valued transmission amplitude, while the complex-valued conversion amplitude is either β (rule I) or $-\beta^*$ (rule II).

III. PREVIOUS TWO-WAVE CONVERSION MODEL

Ray phase-space methods [3] can be used to study mode-conversion scenarios involving intersecting rays that enclose a finite area in two-dimensional ray phase space. The ray phase-space analysis of this mode conversion process reveals the existence of four scenarios based on whether the wave energies have equal or opposite signs, and whether the wave rays are co-propagating or counter-propagating in ray phase space.

A. Connection rules

When mode-coupled rays from different waves intersect in ray phase space in such a way as to enclose a finite area, it is necessary to introduce two different *connection* rules that distinguish between a right-turn conversion and a left-turn conversion (see Fig. 2). The conversion amplitude for a right-turn conversion is β (rule I) while the conversion amplitude for a left-turn conversion is $-\beta^*$ (rule II).

These two connection rules may be combined in matrix form as $\mathbf{Z}^+ = \mathsf{S} \cdot \mathbf{Z}^-$, where $\mathbf{Z}^- = (Z_1^-, Z_2^-)$ and $\mathbf{Z}^+ = (Z_1^+, Z_2^+)$ are incoming $(-)$ and outgoing $(+)$ field amplitudes, and

$$\mathsf{S} = \begin{pmatrix} \tau & \beta \\ -\beta^* & \tau \end{pmatrix} \tag{11}$$

is the S matrix for the mode conversion $1 \leftrightarrow 2$ (where the first and second rows represent the connection rules I and II, respectively). Conservation of energy is now simply expressed as $\det \mathsf{S} = 1$.

While the difference between the two connection rules I and II has no observable consequences for the double-conversion process considered in Sec. II (since both conversions follow the same connection rule), this difference plays a fundamental role in ensuring energy conservation when a finite area is enclosed by intersecting mode-coupled rays [5, 6].

B. Two-wave model

Brizard *et al.* [6, 7] considered a double-conversion scenario in which the ray of a primary wave punctures the dispersion surface of the secondary wave twice due to ray curvature (corresponding to the case of a near-tangential crossing). Specifically, Brizard *et al.* [6, 7] considered the linear interaction between two waves with dispersion curves modeled by intersecting parabolas, with primary and secondary rays that are either co-propagating (Fig. 3) or counter-propagating (Fig. 4).

The creation of an enclosed area by the intersecting parabolas introduces the possibility that the counter-propagating rays may allow energy *recirculation* around a *leaky* cavity (see Fig. 4). Direct numerical integration of the coupled-wave model equations of Ref. [7] yielded excellent agreement with modular eikonal results provided the area enclosed by the intersecting parabolas in ray phase space was large compared to 2π.

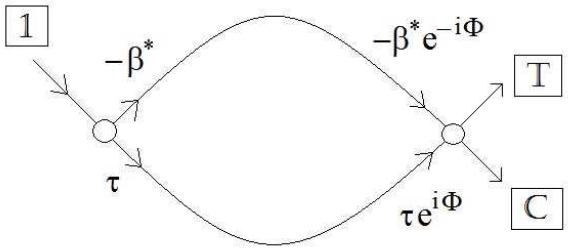

FIG. 3: Co-propagating ray phase-space diagram for intersecting parabolic rays [6, 7]. The transmission (T) and conversion (C) coefficients satisfy the energy conservation law $\mathsf{T} + \mathsf{C} = 1$.

1. *Co-propagating scenarios*

For the co-propagating scenario involving two positive-energy (+) waves (Fig. 3), the transmission and conversion coefficients [7]

$$\mathsf{T}_+(\tau, \Psi_+) \;=\; \left|\tau^2\, e^{i\Phi} \;+\; (\beta^*)^2\; e^{-\,\Phi}\right|^2 \;\equiv\; 1 \;-\; 4\,\tau^2\,\left(1-\tau^2\right)\,\sin^2\Psi_+, \tag{12}$$

$$\mathsf{C}_+(\tau, \Psi_+) \;=\; \left|\tau\,\beta\; e^{i\Phi} \;-\; \tau\,\beta^*\; e^{-i\Phi}\right|^2 \;=\; 4\,\tau^2\,\left(1-\tau^2\right)\,\sin^2\Psi_+ \;\equiv\; 1 \;-\; \mathsf{T}_+(\tau, \Psi_+) \tag{13}$$

are expressed in terms of the single-conversion amplitude τ and the interference phase

$$\Psi_\pm \;\equiv\; \frac{1}{2}\,\oint\, k(x;\eta)\,dx \;\pm\; \varphi \;=\; \Phi \;\pm\; \varphi, \tag{14}$$

which takes into account the area enclosed by the intersecting parabolas (Φ) and the phase (φ) of the conversion amplitude β. Note that the last equality in Eq. (13) expresses the energy conservation law for this scenario. In addition, we note that the conditions $\tau = 1/\sqrt{2}$ and $\sin^2\Psi_+ = 1$ (e.g., $\Psi_+ = \pi/2$) correspond to a situation where the transmission and conversion coefficients are $\mathsf{T}_+(1/\sqrt{2}, \pi/2) = 0$ and $\mathsf{C}_+(1/\sqrt{2}, \pi/2) = 1$, i.e., the cavity allows 100 % conversion under these conditions. The cavity allows 100 % transmission ($\mathsf{T}_+ = 1$ and $\mathsf{C}_+ = 0$), on the other hand, when the interference phase is an integer multiple of π. Hence, as the enclosed area and/or the coupling strength varies, the coefficients T_+ and C_+ alternate between minima and maxima.

When the co-propagating scenario involves a positive-energy wave interacting with a negative-energy wave [$\epsilon = -1$ in Eq. (1)], the transmission and conversion coefficients are expressed in terms of the transmission amplitude $\tau \equiv \exp(+\,\pi\,|\overline{\eta}|^2) > 1$ as [7]

$$\mathsf{T}_-(\tau, \Psi_-) \;=\; 1 \;-\; 4\,\tau^2\,\left(1-\tau^2\right)\,\sin^2\Psi_- \;\equiv\; 1 \;+\; 4\,\tau^2\,\left(\tau^2-1\right)\,\sin^2\Psi_- \;\geq\; 1, \tag{15}$$

$$\mathsf{C}_-(\tau, \Psi_-) \;=\; 4\,\tau^2\,\left(1-\tau^2\right)\,\sin^2\Psi_- \;\equiv\; -\,4\,\tau^2\,\left(\tau^2 \;-\; 1\right)\,\sin^2\Psi_- \;\leq\; 0. \tag{16}$$

where the interference phase Ψ_- is defined in Eq. (14). Hence, while the energy conservation $\mathsf{T}_- + \mathsf{C}_- = 1$ is still satisfied, a negative conversion coefficient ($\mathsf{C}_- < 0$) allows the transmission coefficient $\mathsf{T}_- = 1 + |\mathsf{C}_-| > 1$ to exceed 100 % for this scenario.

2. *Counter-propagating scenario*

The counter-propagating scenario (Fig. 4) allows energy recirculation around a *leaky cavity* in ray phase space. After each cycle, a small amount of energy has *leaked* out of the cavity contributing to the conversion and transmission channels. After N cycles, the amounts of transmitted energy and converted energy out of the cavity are $\sum_{n=1}^{N} \mathsf{T}'_n$ and $\sum_{n=1}^{N} \mathsf{C}'_n$. As $N \to \infty$, all the incident energy has leaked out of the cavity and the transmission and conversion coefficients are

$$(\mathsf{T}', \mathsf{C}') \;\equiv\; \sum_{n=1}^{\infty}\,(\mathsf{T}'_n, \mathsf{C}'_n), \tag{17}$$

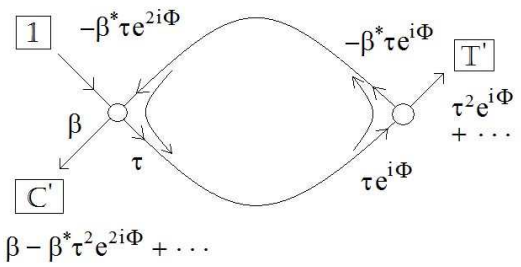

FIG. 4: Counter-propagating ray phase-space diagram for intersecting parabolic rays [6, 7], which allows energy recirculation. The transmission (T') and conversion (C') coefficients satisfy the energy conservation law $\mathsf{T}' + \mathsf{C}' = 1$.

and energy conservation is $\mathsf{T}' + \mathsf{C}' = 1$.

After each cycle, the energy transmitted and converted is expressed in terms of the recirculation coefficient (denoted by the heart symbol)

$$\heartsuit \;\equiv\; (\beta^*)^2\, e^{2i\,\Phi} \;=\; (1-\tau^2)\, e^{2i\,\Psi_-}, \tag{18}$$

which depends on the area enclosed by the intersecting rays and the strength of the wave coupling. The magnitude of the recirculation coefficient $|\heartsuit|$ increases from 0 to 1 as the coupling constant $|\overline{\eta}|$ goes from 0 to infinity.

For the counter-propagating scenario involving two positive-energy (+) waves, the transmission and conversion coefficients are [7]

$$\mathsf{T}'_+(\tau,\Psi_-) \;=\; \left|\tau^2\, e^{i\Phi}\left(1+\heartsuit+\heartsuit^2+\cdots\right)\right|^2 \;\equiv\; \frac{\tau^4}{|1-\heartsuit|^2} \;=\; \frac{\tau^4}{\tau^4 \;+\; 4\,(1-\tau^2)\,\sin^2\Psi_-}, \tag{19}$$

$$\begin{aligned}\mathsf{C}'_+(\tau,\Psi_-) \;&=\; \left|\beta \;-\; \beta^*\,\tau^2\, e^{2i\,\Phi}\left(1+\heartsuit+\heartsuit^2+\cdots\right)\right|^2 \;=\; \left(1-\tau^2\right) \;+\; \frac{\tau^4\,\left(1-\tau^2\right)}{|1-\heartsuit|^2} \;-\; 2\,\mathrm{Re}\left(\frac{\tau^2\,\heartsuit}{1-\heartsuit}\right) \\ &=\; 1 \;-\; \frac{\tau^4}{|1-\heartsuit|^2} \;\equiv\; 1 \;-\; \mathsf{T}'_+(\tau,\Psi_-).\end{aligned} \tag{20}$$

Note that there is a simple relation between the transmission coefficients (15) and (19) expressed as

$$\mathsf{T}_-(\tau,\Psi_-) \;=\; \left[\frac{\tau^{-4}}{\tau^{-4} \;+\; 4\,(1-\tau^{-2})\,\sin^2\Psi_-}\right]^{-1} \;\equiv\; \left[\;\mathsf{T}'_+(\tau^{-1},\Psi_-)\;\right]^{-1}, \tag{21}$$

i.e., the transmission coefficient for the mode conversion of co-propagating positive-energy and negative-energy waves (T_-) is the inverse of the transmission coefficient for the mode conversion of counter-propagating positive-energy waves (T'_+).

When the counter-propagating scenario involves a positive-energy wave interacting with a negative-energy wave (−), the transmission and conversion coefficients are expressed in terms of the transmission amplitude $\tau \equiv \exp(+\,\pi\,|\overline{\eta}|^2) > 1$ as

$$\mathsf{T}'_-(\tau,\Psi_+) \;=\; \frac{\tau^4}{\tau^4 \;-\; 4\,(\tau^2-1)\,\sin^2\Psi_+} \;\equiv\; \left[\mathsf{T}_+(\tau^{-1},\Psi_+)\;\right]^{-1} \;>\; 1, \tag{22}$$

$$\mathsf{C}'_-(\tau,\Psi_+) \;\equiv\; 1 \;-\; \mathsf{T}'_-(\tau,\Psi_+) \;<\; 0. \tag{23}$$

Note that the conditions $\tau = \sqrt{2}$ and $\sin^2\Psi_+ = 1$ now correspond to a situation where the transmission and conversion coefficients both become infinite, i.e., $\mathsf{T}'_- \to \infty$ and $\mathsf{C}'_- \to -\infty$, while still satisfying the energy conservation law $\mathsf{T}'_- + \mathsf{C}'_- = 1$. This scenario was discussed in Ref. [6] in the context of an absolute instability involving the mode conversion between a positive-energy magnetosonic wave and a negative-energy minority-ion Bernstein wave supported by an inverted population of energetic particles.

C. Co-propagating linear three-wave model

The linear three-wave model studied by Liang, Morehead, *et al.* [5] considered a multiple wave-conversion scenario involving an x-propagating (bidirectional) primary wave and two k-propagating secondary (s) and tertiary (t) (unidirectional) waves that are co-propagating along the k-axis within two separate resonance layers (see Fig. 5). In this

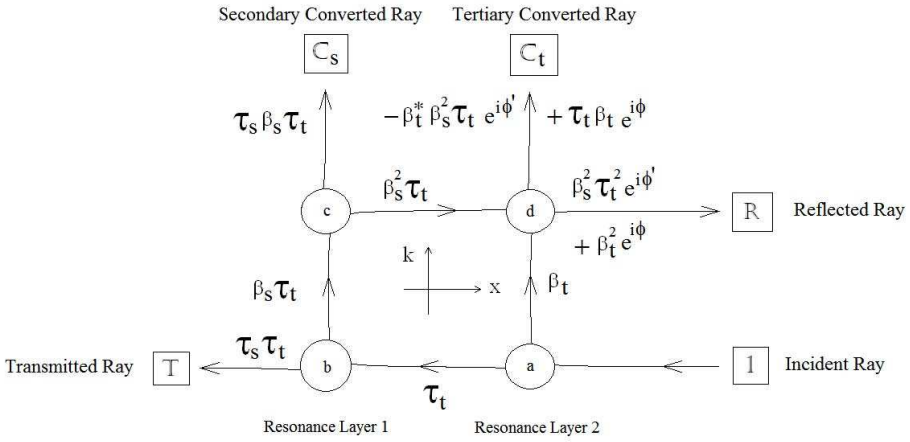

FIG. 5: Ray phase-space diagram (in the limit $\gamma \to 0$) for the co-propagating linear three-wave model of Liang, Morehead, *et al.* [5]. The phase ϕ is the phase accumulated along the segment ad, while the phase ϕ' is the phase accumulated along the segments $abcd$. The reflection coefficient R and the conversion coefficient C_t explicitly exhibit interference effects, while the transmission coefficient T and the conversion coefficient C_s do not exhibit interference. The energy conservation law for this co-propagating three-wave conversion problem is $\mathsf{T} + \mathsf{R} + \mathsf{C}_s + \mathsf{C}_t = 1$.

co-propagating three-wave model, Liang, Morehead, *et al.* [5] introduced four conversion regions (a, b, c, d) that form the vertices of a rectangle in ray phase space produced by the pair-wise intersections of 4 uncoupled rays associated with three waves.

1. *General linear three-wave model*

In a nonuniform plasma with one-dimensional spatial dependence, the linear three-wave conversion process is written in matrix form as

$$\begin{pmatrix} D_A & \eta_s & \eta_t \\ \eta_s^* & D_s & 0 \\ \eta_t^* & 0 & D_t \end{pmatrix} \begin{pmatrix} A \\ B_s \\ B_t \end{pmatrix} \; = \; 0, \tag{24}$$

where the complex-valued fields $A(x)$, $B_s(x)$, $B_t(x)$ represent the primary, secondary, and tertiary waves, respectively. The strengths of the resonant interactions $A \leftrightarrow B_j$ ($j = s$ or t) are expressed by the coupling constants η_j. Note that both the secondary and tertiary waves are coupled only to the primary wave in the present model. Within the eikonal representation, we use the 3×3 dispersion matrix $\mathsf{D}(x, k)$ of Eq. (24) to obtain the dispersion curves $x(k)$ from the dispersion relation

$$\det \mathsf{D}(x, k) \; \equiv \; D_A \, D_s \, D_t \; - \; \left(|\eta_s|^2 \, D_t \; + \; |\eta_t|^2 \, D_s \right) \; = \; 0. \tag{25}$$

The multiple wave-conversion equation (24) introduces the pairwise mode couplings between an x-propagating primary wave A and two k-propagating waves B_s and B_t.

The x-propagating (bidirectional) primary wave A is represented by its dispersion function

$$D_A(k) \; = \; k_0^2 - k^2, \tag{26}$$

while the two k-propagating (unidirectional) secondary and tertiary waves B_s and B_t are represented by their dispersion functions [5] (derived below)

$$\left. \begin{aligned} D_s(x, k) \; &= \; (x + \sigma) - \gamma \, k \\ D_t(x, k) \; &= \; (x - \sigma) - \gamma \, k \end{aligned} \right\}, \tag{27}$$

where $(\sigma, \gamma > 0)$ are model parameters. Here, both the secondary and tertiary waves propagate upward in k-space (see Fig. 5). On the x-axis (at $k = 0$), the rays of the secondary and tertiary waves are separated by the distance $2\,\sigma$.

The choice of the x-space propagation parameter γ for the secondary and tertiary waves does not affect the results of the modular eikonal approach [5]. (Similar wave-conversion models were previously studied by Friedland and Cohen [12], who made use of simple dispersion functions similar to the ones used here.)

The simplified dispersion functions (27) are derived as follows. First, we expand the (physical) dispersion function $D_j(x,k)$ about some point (x_j,k_j) on its dispersion curve $D_j(x,k)=0$, and Taylor expand the function about that point:

$$D_j(x,k) \;=\; \dot{k}_j \;\cdot\; (x-x_j) \;-\; \dot{x}_j \;\cdot\; (k-k_j) + \cdots, \tag{28}$$

where the constant coefficients $\dot{x}_j \equiv -\,\partial_k D_j(x_j,k_j)$ and $\dot{k}_j \equiv \partial_x D_j(x_j,k_j)$ are Hamilton's equations evaluated at (x_j,k_j). Next, we choose $(x_j,k_j)=(\mp\sigma,\,0)$, with $\dot{k}_j=\kappa$ (i.e., the B-wave rays are co-k-propagating, with $\kappa>0$) and $\dot{x}_j=\gamma\,\kappa>0$ (i.e., both B-wave rays are outgoing at $x=+\infty$). Lastly, we rescale the dispersion functions (28) by dividing by κ and obtain the dispersion functions (27) after we drop terms of higher order.

The wave equation (24) satisfies the wave-energy conservation law

$$\frac{d}{dx}\Big[\; J_A(x) \;+\; J_s(x) \;+\; J_t(x) \;\Big] \;=\; 0, \tag{29}$$

where $J_A(x) \equiv \mathrm{Im}(A^*\,dA/dx)$, $J_s(x) \equiv \frac{1}{2}\,\gamma\,|B_s|^2$, and $J_t(x) \equiv \frac{1}{2}\,\epsilon_t\gamma\,|B_t|^2$ are wave-energy flux densities. Here, the tertiary wave-energy flux density J_t is negative when the tertiary wave-energy is negative ($\epsilon_t<0$).

When $\gamma=0$ (i.e., the secondary and tertiary waves are localized within their respective resonance layers), we replace B_j with $-\,[\eta_j^*/(x\pm\sigma)]\,A$ in the wave equation for $A(x)$, and we obtain the extended Budden equation

$$\frac{d^2A}{dx^2} \;+\; \left[\; k_0^2 \;-\; \left(\frac{|\eta_s|^2}{x+\sigma} \;+\; \frac{|\eta_t|^2}{x-\sigma}\right)\;\right] A \;=\; 0. \tag{30}$$

This equation generalizes the standard Budden equation (6) by considering two distinct resonance layers (at $x=\pm\sigma$) instead of a single resonance; note that an explicit solution for $A(x)$ requires a proper handling of the singularities at $x=\pm\sigma$. (A similar extension of the standard Budden problem associated with the presence of sheared flows in magnetized plasmas leads to three resonance layers and a phase-space cavity [13].)

2. Modular eikonal approach

Liang, Morehead, *et al.* [5] then used a modular eikonal approach to show that the reflection coefficient

$$\mathsf{R} \;=\; \left|\beta_t^2\,e^{i\,\phi} \;+\; \beta_s^2\tau_t^2\,e^{i\,\phi'}\right|^2 \;=\; \left(1-\tau_t^2\right)^2 \;+\; \tau_t^4\;\left(1-\tau_s^2\right)^2 \;+\; 2\;\left(1-\tau_t^2\right)\left(1-\tau_s^2\right)\;\tau_t^2\;\cos 2\,\Psi, \tag{31}$$

and the tertiary conversion coefficient

$$\mathsf{C}_t \;=\; \left|\beta_t\tau_t\,e^{i\,\phi} \;-\; \beta_t^*\beta_s^2\tau_t\,e^{i\phi'}\right|^2 \;=\; \left(1-\tau_t^2\right)\;\tau_t^2 \;+\; \left(1-\tau_t^2\right)\left(1-\tau_s^2\right)^2\;\tau_t^2 \;-\; 2\;\left(1-\tau_t^2\right)\left(1-\tau_s^2\right)\;\tau_t^2\;\cos 2\,\Psi \tag{32}$$

explicitly exhibit interference effects, where the interference phase $\Psi \equiv \Phi + \varphi_s - \varphi_t$ depends on the area enclosed by the rectangle ($2\,\Phi \equiv \oint k\,dx = \phi'-\phi$) and the (normalized) coupling constants $(\overline{\eta}_s,\overline{\eta}_t)$, while the transmission and secondary conversion coefficients

$$\left.\begin{array}{rcl} \mathsf{T} &=& \tau_s^2\;\tau_t^2 \\ \mathsf{C}_s &=& \tau_t^2\;\tau_s^2\,(1-\tau_s^2) \end{array}\right\} \tag{33}$$

do not. The energy conservation law for this co-propagating three-wave model is

$$\mathsf{T} \;+\; \mathsf{R} \;+\; \mathsf{C}_s \;+\; \mathsf{C}_t \;=\; 1. \tag{34}$$

Note that the presence of the tertiary wave, viewed here as a perturbation on the two-wave conversion process involving the primary and secondary waves, yields a secondary conversion coefficient $\mathsf{C}_s \equiv \tau_t^2\,\mathsf{C}_B < \mathsf{C}_B$ that is smaller than the standard Budden double-crossing conversion coefficient $\mathsf{C}_B \equiv \tau_s^2\,(1-\tau_s^2)$ for the secondary wave (if the tertiary wave has positive energy $\tau_t<1$).

Lastly, Liang, Morehead, *et al.* [5] obtained excellent agreement between direct numerical integration of the coupled-wave equations and analytical results, thus confirming the validity of the modular eikonal approach when interference effects are present. Note that while the connection rule I is used at each of the conversion regions a, b, and c in Fig. 5, the connection rule II must be used at the conversion region d in order to guarantee the conservation of energy. In fact, the connection rules introduced above confirm the results of Liang, Morehead, *et al.* [5], since the energy conservation law (34) was used in Ref. [5] as a constraint on the coefficients to calculate the tertiary conversion coefficient (32).

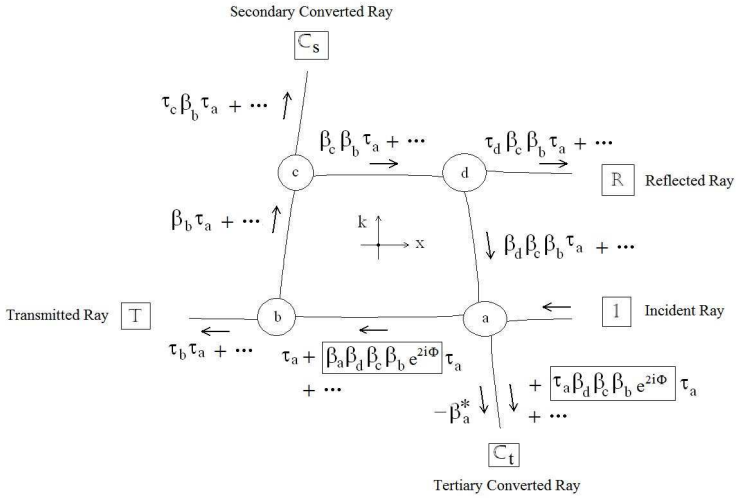

FIG. 6: Counter-k-propagating rays B_s and B_t interacting with x-propagating rays A. Solid lines are dispersion curves representing Eq. (25). The four conversion regions (a, b, c, d) form a quadrangle in ray phase space and arrows show the direction of wave-packet propagation. The net propagation phase $2\,\Phi = \oint k\,dx$ is shown only in the boxed expressions (discussed in the text). For each unit of energy carried by the incoming left-propagating ray A (from $x = +\infty$) introduced at conversion region a, the outgoing left-propagating ray A carries the transmitted energy T (left of conversion region b), the outgoing up-propagating secondary ray B_s carries the converted energy C_s (above conversion region c), the outgoing right-propagating ray A carries the reflected energy R (right of conversion region d), and the outgoing down-propagating tertiary ray B_t carries the converted energy C_t (below conversion region a). Conservation of energy requires that $\mathsf{T} + \mathsf{C}_s + \mathsf{C}_t + \mathsf{R} = 1$.

IV. COUNTER-PROPAGATING LINEAR THREE-WAVE MODEL

In the present Section, we use the modular eikonal approach to study the multiple wave-conversion model based on Eq. (24), in which two counter-propagating positive-energy waves are each interacting resonantly with an x-propagating wave (see Fig. 6); the counter-propagating scenario involving a positive-energy wave and a negative-energy wave is discussed in Sec. VI. These two scenarios are complementary to the co-propagating three-wave model of Liang, Morehead, *et al.* [5], which did not consider the process of energy recirculation. These modifications allow us to investigate the validity of the modular eikonal approach when energy recirculation and interference effects are both present.

The x-propagating (bidirectional) primary wave A is once again represented by the dispersion function (26), while the two k-propagating (unidirectional) secondary and tertiary waves B_s and B_t are now represented by the dispersion functions

$$\left.\begin{array}{rcl} D_s(x,k) &=& (\sigma + x) - \gamma\,k \\ D_t(x,k) &=& (\sigma - x) - \gamma\,k \end{array}\right\}, \tag{35}$$

where $(\sigma, \gamma > 0)$ are model parameters. Here, in contrast to the co-propagating linear three-wave model [5], the secondary wave propagates upward $(+)$ in k-space and the tertiary wave propagates downward $(-)$ in k-space. On the x-axis (at $k = 0$), the rays of the secondary and tertiary waves are separated by the distance $2\,\sigma$ (see Fig. 6). The uncoupled rays cross in phase space at the conversion points

$$\left.\begin{array}{rcl} (x_a, k_a) &=& (\sigma + \gamma\,k_0,\ -k_0) \\ (x_b, k_b) &=& (-\sigma - \gamma\,k_0,\ -k_0) \\ (x_c, k_c) &=& (-\sigma + \gamma\,k_0,\ k_0) \\ (x_d, k_d) &=& (\sigma - \gamma\,k_0,\ k_0) \end{array}\right\}, \tag{36}$$

which define a (symmetric) quadrangle in ray phase space (see Fig. 6). The ray equations ($\dot{x} = -\,\partial_k D$, $\dot{k} = \partial_x D$) yield $(\dot{x}_A,\ \dot{k}_A) = (\pm 2,\ 0)$ and $(\dot{x}_\pm,\ \dot{k}_\pm) = (\gamma,\ \pm 1)$, indicated by arrows in Fig. 6. The use of these simplified dispersion functions, for which the area enclosed by the intersecting rays is easily calculated, allows us to focus our attention on the topology of intersecting counter-propagating rays and the associated interference and recirculation effects.

A. Modular Eikonal Analysis

We now solve the coupled-wave model equations (24), with dispersion functions (26) and (35), by using the modular eikonal approach [5, 6] to calculate the transmission, reflection, and conversion coefficients at the four conversion points (a, b, c, d). This approach makes use of the following single-crossing amplitude transmission and conversion coefficients (τ_s, β_s) and (τ_t, β_t) for the secondary and tertiary waves

$$\left.\begin{array}{rcl} (\tau_a, \beta_a) & = & (\tau_d, \beta_d) \;\equiv\; (\tau_t, \beta_t) \\ (\tau_b, \beta_b) & = & (\tau_c, \beta_c) \;\equiv\; (\tau_s, \beta_s) \end{array}\right\} \tag{37}$$

where $(j = s, t)$

$$\left.\begin{array}{rcl} \tau_j & = & \exp\left(-\,\pi\,|\overline{\eta}_j|^2\right) \\ \beta_j & = & \sqrt{1-\tau_j^2}\;\exp(i\,\varphi_j) \end{array}\right\}, \tag{38}$$

with the conversion phases $\varphi_j \equiv \arg[\Gamma(i|\overline{\eta}_j|^2)]$ and $|\overline{\eta}_j|^2 \equiv |\eta_j|^2/|\{D_A,\, D_j\}|$, where $|\{D_A,\, D_j\}| = 2k_0$ denotes the Poisson bracket of the dispersion functions evaluated at the conversion points.

1. Recirculation

The intersecting rays shown in Fig. 6 exhibit a leaky-cavity feature in ray phase space that allows energy to recirculate around the quadrangle *abcd*. To represent this process, where each conversion along a clockwise recirculation path obeys the connection rule I, we introduce the complex-valued recirculation coefficient

$$\heartsuit \;\equiv\; \beta_d\,\beta_c\,\beta_b\,\beta_a\,e^{2i\Theta} \;=\; \left(1-\tau_s^2\right)\,\left(1-\tau_t^2\right)\,e^{2i\Psi}, \tag{39}$$

with the interference phase [5]

$$\left.\begin{array}{rcl} \Psi & \equiv & \Phi \;+\; \varphi_s \;+\; \varphi_t \\ \Phi & \equiv & 2\,k_0\sigma \;-\; \left(|\overline{\eta}_s|^2 + |\overline{\eta}_t|^2\right)\,\ln(4\,k_0\sigma) \end{array}\right\} \tag{40}$$

expressed as the sum of the propagation phase $2\,\Phi \equiv \oint k\,dx$ (expressed as the sum of the area $4\,k_0\sigma$ enclosed by the uncoupled quadrangle *abcd* and corrections to the uncoupled eikonal phases due to finite coupling constants $\eta_j \neq 0$) and the net conversion phase $\arg(\beta_a\beta_b\beta_c\beta_d) = 2\,(\varphi_s + \varphi_t)$.

We note that the relative simplicity of the recirculation coefficient (39) and interference phase (40) follow from the simplicity of our model presented in Sec. IV.

2. Connection coefficients

Using the modular eikonal approach, we now calculate the connections coefficients involving transmission (T) and reflection (R) associated with the primary wave and conversions to the secondary wave (C_s) and the tertiary wave (C_t). All connection coefficients ($\mathsf{T}, \mathsf{C}_s, \mathsf{C}_t, \mathsf{R}$) are calculated by adding the amplitudes of each successive completed circuit in Fig. 6 and thus they exhibit interference effects that depend on the phase Ψ defined in Eq. (40). These interference effects enter through the recirculation coefficient (39) in two different ways in Fig. 6.

First, successive powers of $\heartsuit$ are added to the zeroth-order amplitudes for the transmission T, secondary conversion C_s, and reflection R coefficients; see the recirculation coefficient $\heartsuit$ in the boxed expression in Fig. 6 between regions a and b. Hence, the transmission coefficient $\mathsf{T} \equiv |A_b^+|^2/|A_a^-|^2$ for the left-propagating primary wave is

$$\mathsf{T} \;=\; \left|\tau_b\,\tau_a\,\left(1 \;+\; \heartsuit \;+\; \heartsuit^2 \;+\; \cdots\right)\right|^2 \;\equiv\; \tau_s^2\tau_t^2\,|1 \;-\; \heartsuit|^{-2}, \tag{41}$$

the secondary conversion coefficient $\mathsf{C}_s \equiv |B_{sc}^+|^2/|A_a^-|^2$ for the upward k-propagating secondary wave is

$$\mathsf{C}_s \;=\; \left|\tau_c\,\beta_b\,\tau_a\,\left(1 \;+\; \heartsuit \;+\; \heartsuit^2 \;+\; \cdots\right)\right|^2 \;=\; \tau_s^2\,(1-\tau_s^2)\,\tau_t^2\,|1 \;-\; \heartsuit|^{-2}, \tag{42}$$

the reflection coefficient $\mathsf{R} \equiv |A_d^+|^2/|A_a^-|^2$ for the right-propagating primary wave is

$$\mathsf{R} \;=\; \left|\tau_d\,\beta_c\,\beta_b\,\tau_a\,\left(1 \;+\; \heartsuit \;+\; \heartsuit^2 \;+\; \cdots\right)\right|^2 \;=\; \tau_t^4\,(1-\tau_s^2)^2\,|1 \;-\; \heartsuit|^{-2}. \tag{43}$$

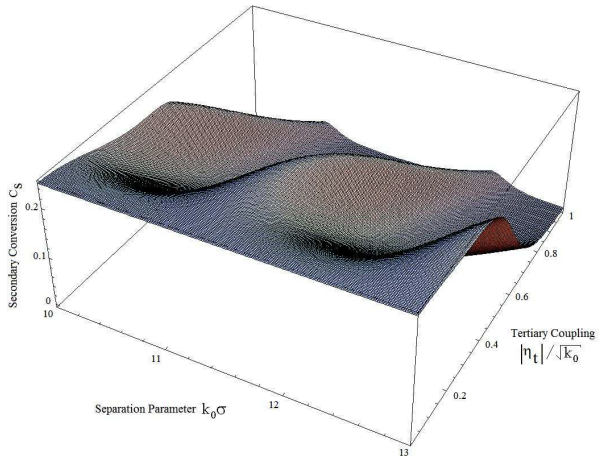

FIG. 7: (Color online) Secondary conversion coefficient (42) as a function of the separation parameter $k_0\sigma$ and the normalized tertiary coupling constant $|\eta_t|/\sqrt{k_0}$, for $\gamma = 1$ and $|\overline{\eta}_s| = [\ln(2)/2\pi]^{\frac{1}{2}}$. At fixed coupling constant $|\overline{\eta}_t|$, the secondary conversion coefficient C_s exhibits interference effects as the separation parameter $k_0\sigma$ is varied and the interference phase (40) passes through integer multiples of π.

In Eqs. (41)-(43), we have used $1 + \heartsuit + \heartsuit^2 + \cdots = (1 - \heartsuit)^{-1}$, since $|\heartsuit| < 1$ for nonzero coupling constants, and

$$|1 \; - \; \heartsuit|^2 \; = \; \left[1 \; - \; \left(1 - \tau_t^2\right) \, \left(1 - \tau_s^2\right)\right]^2 \; + \; 4 \, \left(1 - \tau_t^2\right) \, \left(1 - \tau_s^2\right) \, \sin^2 \Psi. \tag{44}$$

Note that the calculations of the coefficients (41)-(43) involve the connection rule I only.

Second, the recirculation coefficient (39) enters into the tertiary conversion coefficient C_t at lowest order because of the interference between the zeroth-order conversion amplitude $-\beta_a^*$ (i.e., the connection rule II applies at conversion region a for the mode conversion $A \rightarrow B_t$) and the one-circuit amplitude $(\tau_a \, \beta_d \, \beta_c \, \beta_b \, e^{2i\Phi}) \, \tau_a$ (see the boxed expression below region a in Fig. 6). Each additional complete circuit around the quadrangle adds successive powers of $\heartsuit$ to the one-circuit amplitude. Hence, the tertiary conversion coefficient $\mathsf{C}_t \equiv |B_{ta}^+|^2/|A_a^-|^2$ for the downward k-propagating tertiary wave is

$$\begin{aligned} \mathsf{C}_t \; &= \; \left|- \beta_a^* + \left(\tau_a \, \beta_d \, \beta_c \, \beta_b \, e^{2i\Phi}\right) \, \tau_a \left(1 + \heartsuit + \heartsuit^2 + \cdots\right)\right|^2 \\ &= \; \left(1 - \tau_t^2\right) \left\{1 \; + \; |1 \; - \; \heartsuit|^{-2} \left[\; \tau_t^2 \, \left(1 - \tau_s^2\right)^2 \, \left(2 - \tau_t^2\right) \; - \; 2 \, \tau_t^2 \, \left(1 - \tau_s^2\right) \, \cos 2 \, \Psi \right] \right\}. \end{aligned} \tag{45}$$

It is now clear that, in contrast to the co-propagating scenario considered by Liang, Morehead, *et al.* [5], all coefficients (41)-(43) and (45) exhibit interference effects

The connection coefficients (41)-(45) depend on the model parameter σ and the coupling constants $|\overline{\eta}_j|$ but not on the propagation parameter γ, which represents a simplifying property of the symmetric-quadrangle model used here (since the enclosed area is independent of γ). They also satisfy the energy conservation law

$$1 \; = \; \mathsf{T} \; + \; \mathsf{C}_s \; + \; \mathsf{C}_t \; + \; \mathsf{R}, \tag{46}$$

which follows from the wave energy conservation law (29). The foundations of the exact energy conservation law (46) are based on the existence of the two distinct connection rules I and II.

Figure 7 shows a plot of the secondary conversion coefficient (42) as a function of the separation parameter $k_0\sigma$ and the normalized tertiary coupling constant $|\overline{\eta}_t|$, for $\gamma = 1$ and $|\overline{\eta}_s| = [\ln(2)/2\pi]^{\frac{1}{2}}$ (where the standard Budden conversion coefficient $\mathsf{C}_B \equiv \tau_s^2 \, (1 - \tau_s^2)$ reaches its maximum at $\frac{1}{4}$); the other connection coefficients $(\mathsf{T}, \mathsf{C}_t, \mathsf{R})$ exhibit similar interference effects while satisfying the conservation law (46).

We make three remarks concerning our connection coefficients (41)-(45). First, the standard Budden coefficients [3] are recovered from Eqs. (41)-(45) in the absence of the tertiary wave ($\eta_t = 0$), so that $\tau_t = 1$ and $\beta_t = 0 = \heartsuit$. Second, as the tertiary coupling constant $|\eta_t| \rightarrow \infty$, the tertiary conversion coefficient $\mathsf{C}_t \rightarrow 1$ and the remaining coefficients $(\mathsf{T}, \mathsf{C}_s, \mathsf{R}) \rightarrow 0$ as can be seen in Fig. 7 (where C_s becomes very small as $|\overline{\eta}_t| > 1$). Third, the use of a generic asymmetric-quadrangle model would only shift the minima and maxima in the connection coefficients and preserve the interference effects associated with recirculation. The simplifying features of our multiple wave-conversion model developed in Sec. IV allowed us to derive explicit analytical results for the connection coefficients $(\mathsf{T}, \mathsf{C}_s, \mathsf{C}_t, \mathsf{R})$.

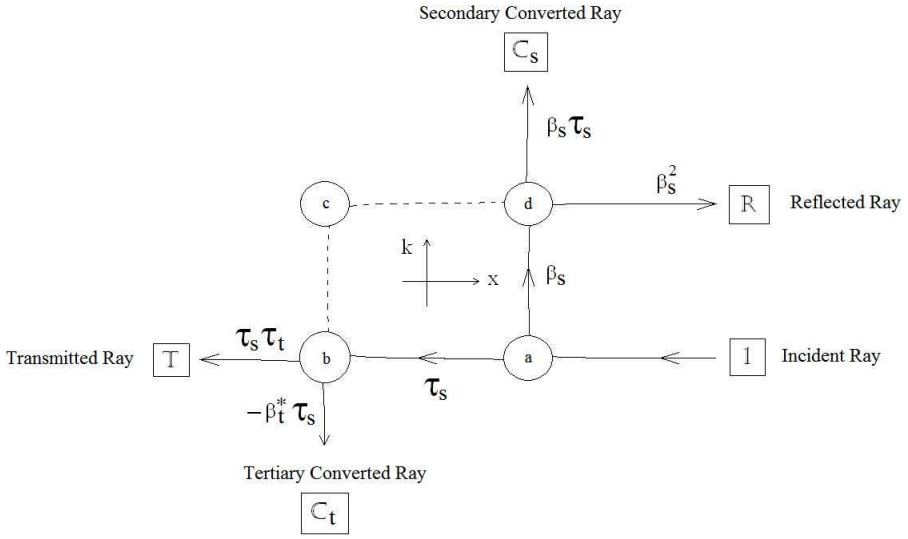

FIG. 8: Reversed counter-propagating three-wave model in which recirculation is no longer possible.

3. Reversed counter-propagating three-wave model

The scenario considered in Fig. 6 assumes that the incoming x-propagating primary wave interacts with the downward k-propagating tertiary wave first before interacting with the upward k-propagating secondary wave. We note that all interference effects disappear in our model when the order of the two counter-k-propagating secondary and tertiary waves is reversed (i.e., we assign negative values to the separation parameter $k_0\sigma$) since recirculation is then no longer possible (see Fig. 8).

In this reversed scenario, the connection coefficients (41)-(45) simply become

$$\left.\begin{array}{rcl} \mathsf{T} &=& \tau_s^2\tau_t^2 \\ \mathsf{C}_s &=& \tau_s^2\,(1-\tau_s^2) \\ \mathsf{R} &=& (1-\tau_s^2)^2 \\ \mathsf{C}_t &=& \tau_s^2\,(1-\tau_t^2) \end{array}\right\}, \tag{47}$$

respectively, which still satisfy the conservation law (46).

The reversed scenario shown in Fig. 8 may be viewed as a combination of a standard double-conversion Budden problem involving the primary and secondary waves, with coefficients $\mathsf{T}_B = \mathsf{T} + \mathsf{C}_t \equiv \tau_s^2$, $\mathsf{C}_B = \mathsf{C}_s$, and $\mathsf{R}_B = \mathsf{R}$, and an isolated single-conversion problem involving the primary and tertiary waves.

V. NUMERICAL ANALYSIS

We now compare the analytical results presented in Sec. IV with the direct numerical integration of the coupled-wave differential equations (24) with the propagating parameter $\gamma = 1$ and the normalized coupling constants $|\overline{\eta}_s| = [\ln(2)/2\pi]^{\frac{1}{2}} = |\overline{\eta}_t|$, and the boundary conditions corresponding to only a left-propagating A-wave with eikonal amplitude A_0 at $x = -\infty$ (and no other waves). With these boundary conditions, the energy conservation law (29) yields

$$-\,k_0\,|A_0|^2 \;=\; k_0\left(|A_R(+)|^2 - |A_L(+)|^2\right) \;+\; \sum_j\, J_j(+),$$

where $A_{R,L}(+)$ denote the eikonal amplitudes of the right (R) and left (L) propagating A-waves at $x = +\infty$. By comparing this equation with Eq. (46), we define the numerical coefficients

$$\left.\begin{array}{rcl} \mathsf{T} &=& |A_0|^2/|A_L(+)|^2 \\ \mathsf{C}_j &=& J_j(+)/(k_0|A_L(+)|^2) \\ \mathsf{R} &=& |A_R(+)|^2/|A_L(+)|^2 \end{array}\right\}. \tag{48}$$

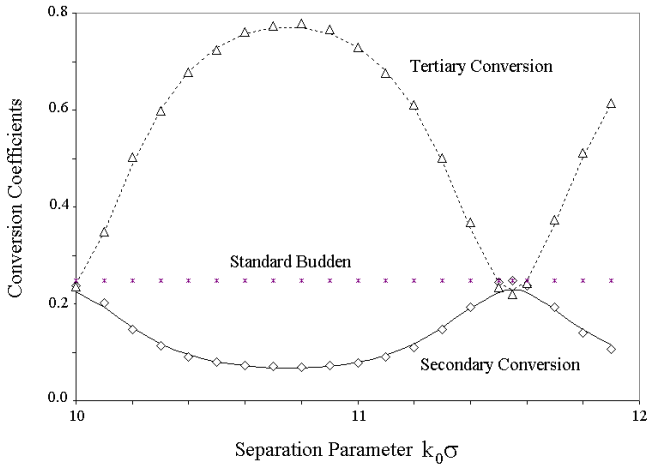

FIG. 9: Conversion coefficients C_s and C_t versus separation parameter $k_0\sigma$ for $\gamma = 1$ and $|\overline{\eta}_s| = |\overline{\eta}_t| = [\ln(2)/2\pi]^{\frac{1}{2}}$. The solid and dotted lines represent the theoretical formulas (42) and (45), respectively, and the symbols $\diamondsuit$ and $\triangle$ represent numerical results for C_s and C_t, respectively. The standard Budden conversion $\mathsf{C}_B = \frac{1}{4}$, corresponding to $\eta_t = 0$ and $|\overline{\eta}_s| = [\ln(2)/2\pi]^{\frac{1}{2}}$, is also shown (represented by a horizontal set of $\times$ symbols).

The conversion coefficients C_j are shown in Fig. 9, where excellent agreement is found between numerical results (48) and the analytical conversion coefficients (42) and (45). The value of the conversion coefficient $\mathsf{C}_B = \frac{1}{4}$ corresponding to the standard Budden problem (with $\eta_t = 0$) is also shown and it is clearly seen that the presence of the counter-propagating tertiary wave reduces the conversion to the secondary wave, i.e., $\mathsf{C}_s < \mathsf{C}_B$. We note that the modular eikonal analysis [5, 6] is valid only when the area (approximately $4\,k_0\sigma$) enclosed by the quadrangle in Fig. 6 is large enough compared to 2π (i.e., the separation σ is large compared to the wavelength).

VI. NEGATIVE-ENERGY TERTIARY WAVE

In Sec. III B, we showed that the co-propagating and counter-propagating scenarios associated with a negative-energy wave [6, 7] supported by an inverted population of energetic particles allow for the transmission coefficient to exceed unity [see Eqs. (15) and (22)]. In the linear three-wave model presented in Sec. IV, the sign of the tertiary wave is determined by the sign of $\partial D_t/\partial\omega$, which may be negative for some energetic-particle distributions in fusion plasmas. In the case of a negative-energy tertiary wave, the tertiary-wave transmission coefficient amplitude exceeds unity:

$$\tau_t \;\equiv\; \exp(+\,\pi|\overline{\eta}_t|^2) \;>\; 1. \tag{49}$$

The denominator (44) in the secondary conversion coefficient (42) is replaced with

$$|1 \;-\; \heartsuit|^2 \;=\; \left[1 \;+\; \left(\tau_t^2 - 1\right)\,\left(1 - \tau_s^2\right)\right]^2 \;-\; 4\,\left(\tau_t^2 - 1\right)\,\left(1 - \tau_s^2\right)\,\sin^2\Psi', \tag{50}$$

where the interference phase is now $\Psi' \equiv \Phi + \varphi_s - \varphi_t$. The denominator (50) can now vanish for $\sin^2\Psi' = 1$ when $\tau_t^2 = (2 - \tau_s^2)/(1 - \tau_s^2)$ or when the normalized tertiary coupling constant has the squared magnitude

$$|\overline{\eta}_t|^2 \;=\; \frac{1}{2\pi}\;\ln\left(\frac{1-\tau_s^2}{2-\tau_s^2}\right), \tag{51}$$

e.g., $|\overline{\eta}_t| = [\ln(3)/2\pi]^{-\frac{1}{2}}$ for $|\overline{\eta}_s| = [\ln(2)/2\pi]^{\frac{1}{2}}$.

By substituting Eq. (49) into Eq. (45), the tertiary conversion coefficient becomes negative, $\mathsf{C}_t < 0$, so that the secondary (bulk-ion) conversion coefficient C_s can exceed unity (see Fig. 10) even as the conservation law (46) is preserved. This is also easily understood from the fact that the energy conservation law (29), now expressed as

$$\frac{d}{dx}\Big[\;J_A(x) \;+\; J_s(x) \;-\; |J_t(x)|\;\Big] \;=\; 0, \tag{52}$$

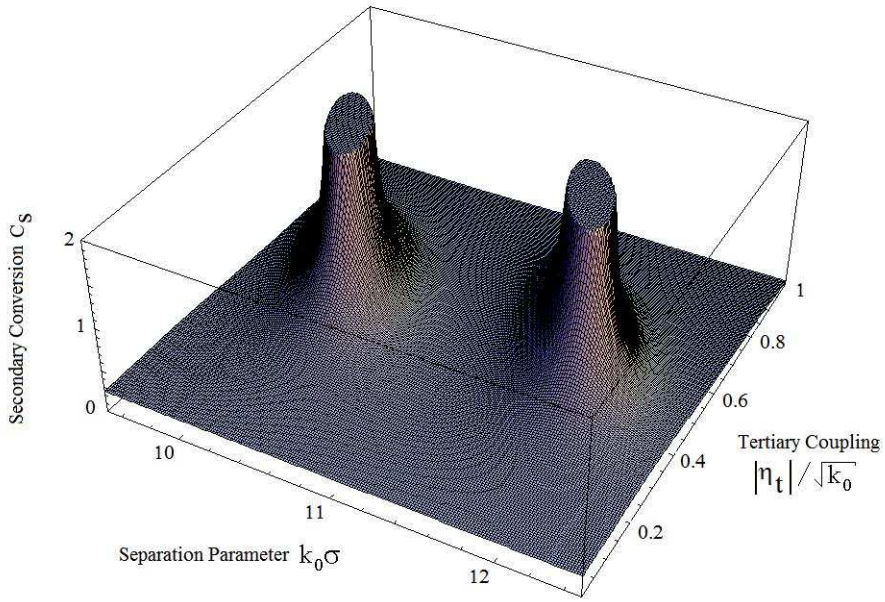

FIG. 10: (Color online) Secondary conversion coefficient (42) as a function of the separation parameter $k_0\sigma$ and the normalized tertiary coupling constant $|\eta_t|/\sqrt{k_0}$, for $\gamma = 1$ and $|\overline{\eta}_s| = [\ln(2)/2\pi]^{\frac{1}{2}}$. Because an inverted energetic-particle population may support a negative-energy tertiary wave, which yields $\exp(+\pi|\overline{\eta}_t|^2) \equiv \tau_t^{-1} > 1$, the tertiary conversion coefficient (45) becomes negative, while the other coefficients $(\mathsf{T}, \mathsf{R}, \mathsf{C}_s)$ may exceed unity. (The Figure shows the secondary conversion C_s arbitrarily truncated at 2.)

allows for all terms to grow [6], since the tertiary wave-energy flux density is now negative. In this process, energy could be extracted from a negative-energy wave supported by an inverted energetic-particle population and be transfered directly to the bulk-ion population (heated by the secondary wave).

This indirect transfer of energy from the energetic particles to the bulk ions, which represents a new form of alpha-channeling process (i.e., the direct transfer of energy from fusion products to bulk ions without the intermediary role of electrons [14, 15]), may then significantly increase the rf power absorption by bulk ions in burning plasmas.

VII. CONCLUSIONS

The purpose of the present work is to investigate how the standard two-wave conversion process associated with heating and/or driving current in a magnetized fusion plasma would be affected by the presence of a tertiary wave able to interact linearly with the primary wave.

The simple topology of the one-dimensional multiple wave-conversion model presented here demonstrates that the mode conversion between primary and secondary waves can be significantly modified by the presence of a tertiary wave. By focusing our attention on the topology of intersecting rays in two-dimensional phase space, our model is constructed to investigate quantitatively the interference effects associated with energy recirculation. The simplicity of our model also allowed us to validate the modular eikonal approach by direct comparison of analytic and numerical results.

Two scenarios are investigated with our conceptual topological model. First, when the positive-energy secondary and tertiary waves are counter-propagating in k-space and interact linearly with the primary wave, we show that interference and energy-recirculation effects in ray phase space lead to a degradation of energy conversion from the primary wave to the secondary wave (see Fig. 9). Second, when the tertiary wave has negative energy, the wave-energy conservation law (52) allows unbounded energy conversion to the secondary wave (see Fig. 10). This second scenario could potentially have important applications in the development of burning fusion plasmas.

Future work will include the development of more realistic models (including specific wave types used in rf heating or current drive in fusion plasmas) in multi-dimensional spatial geometry, as well as the investigation of the new alpha-channeling process involving a negative-energy tertiary wave supported by an inverted energetic-particle population.

Acknowledgments

This work was supported by U.S. DoE under grant No. DE-AC03-76SFOO098. One of us (E.R.T.) also acknowledges support from U.S. DoE under grant No. DE-FG02-96ER54344 and NSF-DoE under contract No. DE-FG02-06ER54885.

---

[1] M. J. Mantsinen, L.-G. Eriksson, E. Gauthier, G. T. Hoang, E. Joffrin, R. Koch, X. Litaudon, A. Lyssoivan, P. Mantica, M. F. F. Nave, J.-M. Noterdaeme, C. C. Petty, and S. E. Sharapov, Plasma Phys. Control. Fusion **45**, A445 (2003).
[2] E. F. Jaeger, L. A. Berry, E. F. D'Azevedo, R. F. Barrett, S. D. Ahern, D. W. Swain, D. B. Batchelor, R. W. Harvey, J. R. Myra, D. A. DiIppolito, C. K. Phillips, E. Valeo, D. N. Smithe, P. T. Bonoli, J. C. Wright, and M. Choi, Phys. Plasmas **15**, 072513 (2008).
[3] E. R. Tracy and A. N. Kaufman, Phys. Rev. E **48**, 2196 (1993).
[4] E. R. Tracy, A. N. Kaufman, and A. J. Brizard, Phys. Plasmas **10**, 2147 (2003).
[5] Y.-M. Liang, J. J. Morehead, D. R. Cook, T. Flå, and A. N. Kaufman, Phys. Lett. A **193**, 82 (1994).
[6] A. J. Brizard, J. J. Morehead, A. N. Kaufman, and E. R. Tracy, Phys. Rev. Lett. **77**, 1500 (1996).
[7] A. J. Brizard, J. J. Morehead, A. N. Kaufman, and E. R. Tracy, Phys. Plasmas **5**, 45 (1998).
[8] D. R. Cook, W. G. Flynn, J. J. Morehead, and A. N. Kaufman, Phys. Lett. A **174**, 53 (1993).
[9] A. A. Galeev and R. S. Sagdeev, *Nonlinear plasma theory*, Rev. Plasma Phys. **7**, M. A. Leontovich, ed. (Consultants Bureau, NY 1979).
[10] A. J. Brizard and A. N. Kaufman, Phys. Rev. Lett. **76**, 1639 (1996).
[11] A. J. Brizard and A. N. Kaufman, Phys. Plasmas **3**, 64 (1996).
[12] L. Friedland and D. Cohen, Phys. Fluids B **4**, 24 (1992).
[13] A. N. Kaufman, A. J. Brizard, and E. R. Tracy, in *16th Topical Conference on Radio Frequency Power in Plasmas* (AIP Conference Proceedings No. 787, New York, 2005), 146-149.
[14] M. C. Herrmann and N. J. Fisch, Phys. Rev. Lett. **79**, 1495 (1997).
[15] N. J. Fisch and M. C. Herrmann, Plasma Phys. Control. Fusion **41**, A221 (1999).